

Scientific paper

Cyclic Behavior of Interfaces for Seismically Retrofitted RC Buildings

Taizo Yamada¹, Yuya Takase^{2*} and Takahide Abe³

Received 15 November 2022, accepted 31 January 2023

doi:10.3151/jact.21.92

Abstract

In seismically retrofitted reinforced concrete (RC) structures, new members are connected to existing members using interfaces with roughened surfaces and post-installed dowel bars. During an earthquake, the interfaces are subjected to cyclic shear and normal stresses. Therefore, the structural design of interfaces is essential. In a previous study, normal and shear loads were applied to interface specimens. Moreover, a shear strength estimation method was proposed; however, the cyclic behavior was not discussed. This paper presents a cyclic model of the roughened surface in retrofitted RC structures. First, an envelope model was constructed using the previous shear strength estimation method and Saenz model, a constitutive law of concrete. Subsequently, the cyclic rules were modeled. Moreover, a previous dowel model was incorporated into the proposed cyclic model to estimate the test results. Finally, the proposed model provided reasonably estimated test results; the average ratio of the test results to the model results was 1.04. In addition, as δ increased, the effect of the dowel bar intensified in terms of shear.

1. Introduction

Several seismically low structures have been retrofitted to prevent the collapse of earthquakes. In retrofitted reinforced concrete (RC) structures, new members should be rigidly connected to existing members. A roughened surface and post-installed dowel bar were applied to interfaces. Generally, for the seismic retrofitting of existing buildings, concrete surfaces are roughened using a vibration hammer (Takase and Yamada 2022). **Figure 1** illustrates an example of an interface for seismically retrofitted RC buildings. During an earthquake, the interfaces are subjected to cyclic shear and normal forces; therefore, estimating the cyclic behavior is essential for a safe structural design. Furthermore, according to the Japanese guidelines (JBDPA 2007), a slip must be less than 2 mm.

Studies of interfaces with roughened surfaces and dowel bars have been conducted since the 1960s. Mattock proposed the shear-friction theory. According to the theory, the yield strength of a bar and the compressive normal stress on a roughened surface equilibrate; based on this condition, the shear strength was calculated. Aggregate interlocking has been considered since the 1980s. Walraven (1981) and Walraven and Reinhardt (1981) modeled a crack surface with aggregates regarded as spherical bodies. Bujadaham and Maekawa (1992a,

1992b) presented a contact density model using a contact density function that expresses one of the shape properties of the local crack. Although studies on aggregate interlocking belong to a classical research topic, the modeling approach has developed in the recent years (Figueira *et al.* 2020). In addition, Zhang *et al.* (2009) studied the shear resistance of roughened surfaces of concrete and polymer cement mortar.

Many researchers have studied dowel action. Friberg (1938) initiated studies on dowel action. Thereafter, Vintzēleou and Tassios (1986) proposed the famous formula for dowel. Sorensen (2017) introduced catenary actions to dowels. Moreover, Maekawa and Qureshi (1997) combined dowel action and aggregate interlocking; subsequently, cyclic behaviors were estimated by Maekawa and Fukuura (2008). However, the behavior under tensile normal stress was not studied, and the surface was not roughened by a vibration hammer. Interfaces with dowel bars and roughened surfaces were also used for precast structures (Ghayeb *et al.* 2020).

Moreover, the authors studied a roughened surface that was manufactured using a vibration hammer. Isozaki *et al.* (2018) proposed an envelope model for a roughened surface using the contact density model, a constitutive model for cracked surfaces (Bujadaham and Maekawa 1992a, 1992b). Additionally, a simple envelope model was constructed to estimate the mechanical behavior under combined stress (Katagiri *et al.* 2019; Yamada *et al.* 2022). The cyclic model of post-installed anchors was proposed in previous studies (Takase *et al.* 2013, 2018, 2019; Matsunaga *et al.* 2021, 2022); however, a cyclic model for roughened surfaces has not been proposed yet. For applying the constitutive model to finite element analysis and analyzing structures subjected to seismic loads, a cyclic model of the roughened surface is also re-

¹Graduate Student, College of Environmental Technology, Muroran Institute of Technology, Muroran, Japan.

²Associate Professor, College of Design and Manufacturing Technology, Muroran Institute of Technology, Muroran, Japan. *Corresponding author, E-mail: y.takase@mmm.muroran-it.ac.jp

³Manager, Institute of Technology, Tobishima Corporation, Noda, Japan.

Table 1 Parameters of the test. D, R, T (in the first column) indicate the dowel bar, roughened ratio, and tensile stresses, respectively. d_d , r_{rc} , and r_N . d_h , f_y , and E_s are the diameter of the boring hole (mm), the yield strength (N/mm²), and the Young's modulus (kN/mm²) of dowel bar, respectively. f_c , and E_c are the compressive strength and the Young's modulus of concrete, while f_g , and E_g are the compressive strength and the Young's modulus of grout, respectively. D_{max} is the maximum depth of concavity of concrete (mm).

Specimen ID	r_N	r_{rc}		Dowel bar				Concrete		Grout		D_{max}
		Target	Measured	d_d	d_h	f_y	E_s	f_c	E_c	f_g	E_g	
D13R01T ₀₀₀	0.00	0.1	0.098	13	16	381	171	23.0	17.5	65.6	26.4	12.0
D13R01T ₀₃₃	0.33	0.1	0.106	13	16	381	171	23.0	17.5	65.6	26.4	11.5
D13R01T ₀₆₆	0.66	0.1	0.107	13	16	381	171	23.0	17.5	65.6	26.4	11.0
D13R02T ₀₀₀	0.00	0.2	0.194	13	16	381	171	23.0	17.5	65.6	26.4	12.0
D13R02T ₀₃₃	0.33	0.2	0.210	13	16	381	171	23.0	17.5	65.6	26.4	12.0
D13R02T ₀₆₆	0.66	0.2	0.199	13	16	381	171	23.0	17.5	65.6	26.4	12.5
D13R03T ₀₀₀	0.00	0.3	0.300	13	16	381	171	23.0	17.5	65.6	26.4	11.0
D13R03T ₀₃₃	0.33	0.3	0.318	13	16	381	171	23.0	17.5	65.6	26.4	18.0
D13R03T ₀₆₆	0.66	0.3	0.304	13	16	381	171	23.0	17.5	65.6	26.4	12.0
D16R01T ₀₀₀	0.00	0.1	0.093	16	22	387	175	20.8	16.4	62.9	24.4	11.5
D16R01T ₀₃₃	0.33	0.1	0.094	16	22	387	175	20.8	16.4	62.9	24.4	11.3
D16R01T ₀₆₆	0.66	0.1	0.106	16	22	387	175	20.8	16.4	62.9	24.4	13.0
D16R02T ₀₀₀	0.00	0.2	0.196	16	22	387	175	20.8	16.4	62.9	24.4	13.0
D16R02T ₀₃₃	0.33	0.2	0.199	16	22	387	175	20.8	16.4	62.9	24.4	11.5
D16R02T ₀₆₆	0.66	0.2	0.210	16	22	387	175	20.8	16.4	62.9	24.4	13.0
D16R03T ₀₀₀	0.00	0.3	0.301	16	22	387	175	20.8	16.4	62.9	24.4	12.9
D16R03T ₀₃₃	0.33	0.3	0.294	16	22	387	175	20.8	16.4	62.9	24.4	15.0
D16R03T ₀₆₆	0.66	0.3	0.292	16	22	387	175	20.8	16.4	62.9	24.4	15.0
D19R01T ₀₀₀	0.00	0.1	0.095	19	25	391	176	23.0	17.5	65.6	26.4	12.0
D19R01T ₀₃₃	0.33	0.1	0.102	19	25	391	176	23.0	17.5	65.6	26.4	13.0
D19R01T ₀₆₆	0.66	0.1	0.096	19	25	391	176	23.0	17.5	65.6	26.4	11.0
D19R02T ₀₀₀	0.00	0.2	0.215	19	25	391	176	23.0	17.5	65.6	26.4	13.0
D19R02T ₀₃₃	0.33	0.2	0.203	19	25	391	176	23.0	17.5	65.6	26.4	13.5
D19R02T ₀₆₆	0.66	0.2	0.204	19	25	391	176	23.0	17.5	65.6	26.4	10.5
D19R03T ₀₀₀	0.00	0.3	0.307	19	25	391	176	23.0	17.5	65.6	26.4	14.5
D19R03T ₀₃₃	0.33	0.3	0.304	19	25	391	176	23.0	17.5	65.6	26.4	13.0
D19R03T ₀₆₆	0.66	0.3	0.304	19	25	391	176	23.0	17.5	65.6	26.4	12.5
Ave.												12.6

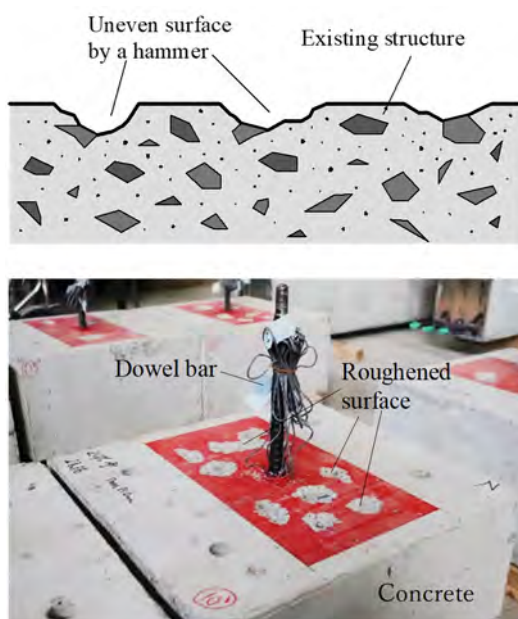


Fig. 1 Examples of interfaces (Takase and Yamada 2022).

quired. In addition, for structural designs of seismic retrofitted structures, envelope and cyclic models for interfaces are useful. In the previous study (Takase and Yamada 2022), the interface specimens were subjected to shear and normal loads. Moreover, a shear strength expression was proposed. However, the cyclic behavior was not discussed. Therefore, in this study, envelope and cyclic behavior models of a roughened surface were proposed; subsequently, the model's accuracy was investigated by using the previous test results.

2. Shear loading test

In this study, previous test results (Takase and Yamada 2022) were used for comparison with the proposed model results. This section briefly explains the shear loading tests.

Table 1 lists the test parameters and material properties of dowel bars, concrete, and grout. In the test, the roughened ratio r_{rc} , diameter of the dowel bar d_d , and tensile ratio r_N were used as the test parameters. r_{rc} is the ratio of the roughened surface to the interface area A_j obtained by the following equation:

$$r_{rc} = \frac{A_{hrc}}{A_j} \quad (1)$$

where A_{hrc} is the horizontal projection area of the uneven surface.

According to Abe *et al.* (2020), the shear strength of the roughened surface is affected by r_{rc} , whereas the effect of D_{max} is weak. Hence, in this study, r_{rc} was used as one of the test parameters. The values of r_{rc} were set to 0.1, 0.2, and 0.3; therefore, the failure mode was bearing failure (Isozaki *et al.* 2018). The ratio of the tensile stress to the yield stress of the dowel bar (r_N) was set to 0.00, 0.33, and 0.66 for $d_d = 13$, 16, and 19 mm, respectively. Concrete with $f_c = 20$ N/mm² was used in this study. The material tests were based on JIS standards (JSA 2011, 2018).

Figure 2 shows an outline of the shear loading test. The specimens consisted of concrete and grout blocks with dimensions of 440 mm × 460 mm × 250 mm and 375 mm × 200 mm × 190 mm, respectively. Because the concrete was cast vertically, the surfaces of the interface sides exhibited a smooth finish with plywood as the formwork. In addition, the surface was greased; therefore, friction was negligible.

The ratios of the longitudinal and transverse bars, indicated as p_g and p_w , were determined to model a normal RC beam and a joint; subsequently, p_g and p_w were 0.74%

and 0.28% for the concrete block and 0.75% and 0.76% for the grout block. After curing for 28 days, when the concrete hardened adequately, the concrete surfaces were roughened, and the anchor bolts were adhered. A hammer and a diamond core drill were used to manufacture the joint surfaces. An epoxy adhesive was applied to the anchors.

The loading setup shown in **Fig. 2** was used for this test. Two 150 kN screw jacks and a 500 kN hydraulic jack were employed in the setup. Four displacement sensors were used to measure the slip δ and opening w . The measured values of w were used for a proportional-integral-derivative (PID) auto-control system, such that the surface moved horizontally during shear loading. Thus, the two load cells were attached to the screw jacks. When the loading beam, as shown in **Fig. 2**, was forced to be parallel based on the PID auto-control, subsequently, the values of the load cells were different. Therefore, the loading beam was vertically moved with the sum of the load cells as the target normal load. The screw jacks were translated by the servo motors, which were controlled by the voltage. For this control, the PID auto-control system was constructed on LabVIEW. **Figure 3** illustrates examples of the normal force-shear displacement (N - δ) relations. As observed in **Fig. 3**, the values of N mostly coincide with the target normal force. Thus, the system had high control accuracy. The steel arm was attached to the steel

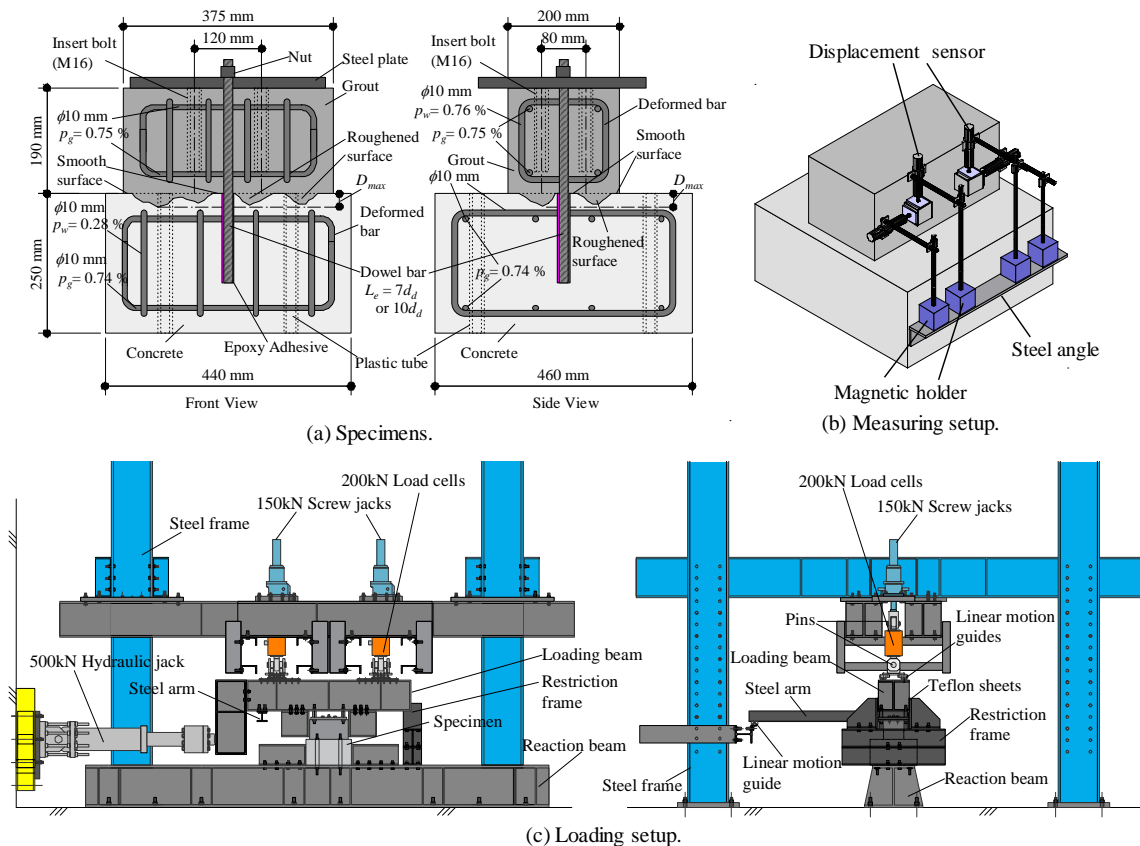


Fig. 2 Outlines of the test.

frame via a linear motion guide, which means it can move horizontally in the shear direction. Furthermore, the out-of-plane deformation of the loading beam was prevented using the steel arm and restriction steel frame displayed in Fig. 2(c).

A static shear load was applied to the specimens at a loading rate of 0.02-0.04 mm/s. The loading cycle was ± 0.125 , ± 0.25 , ± 0.50 , ± 1.0 , ± 1.5 , ± 2.0 , ± 3.0 , ± 4.0 , ± 6.0 , and ± 8.0 mm.

3. Test results

The test results are presented in the following section.

3.1 Failure mode

Figure 4 shows the failure modes. As mentioned in the

previous papers (Isozaki *et al.* 2018; Takase and Yamada 2022), the failure mode of the roughened surface can be classified as bearing and shear failures. The sides of the uneven surfaces are vertically damaged in the bearing failure, as shown in Fig. 4(b). The uneven surfaces of both concrete and grout are horizontally failed in the shear failure; therefore, in the shear failure, the fractured grout remained in the concavity of concrete, as shown in Fig. 4(c).

Observing Fig. 4(a), after loading, the uneven area was larger than that before loading. Moreover, in the concavity of concrete, the fractured grout rarely remained; therefore, the fracture mode of the test was the bearing failure.

3.2 Maximum shear load and slip

Subsequently, the maximum shear loads and the slips are

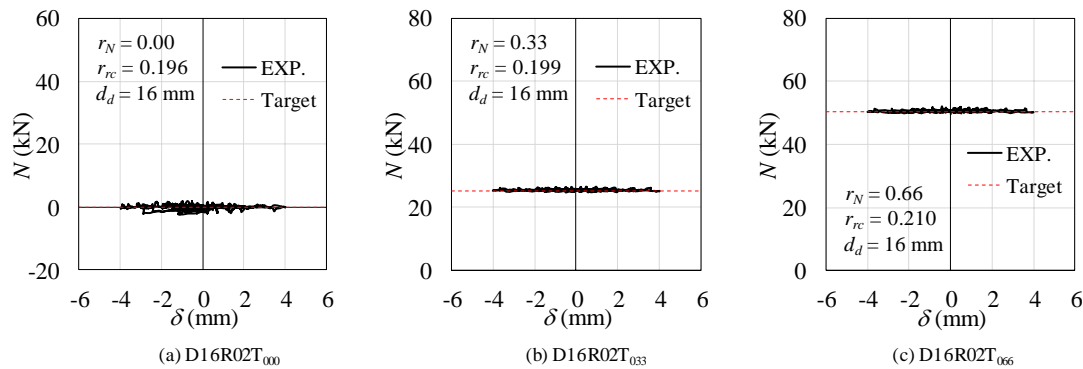


Fig. 3 Examples of N - δ relationships, with $d_d = 16$ mm and $r_{rc} = 0.2$.

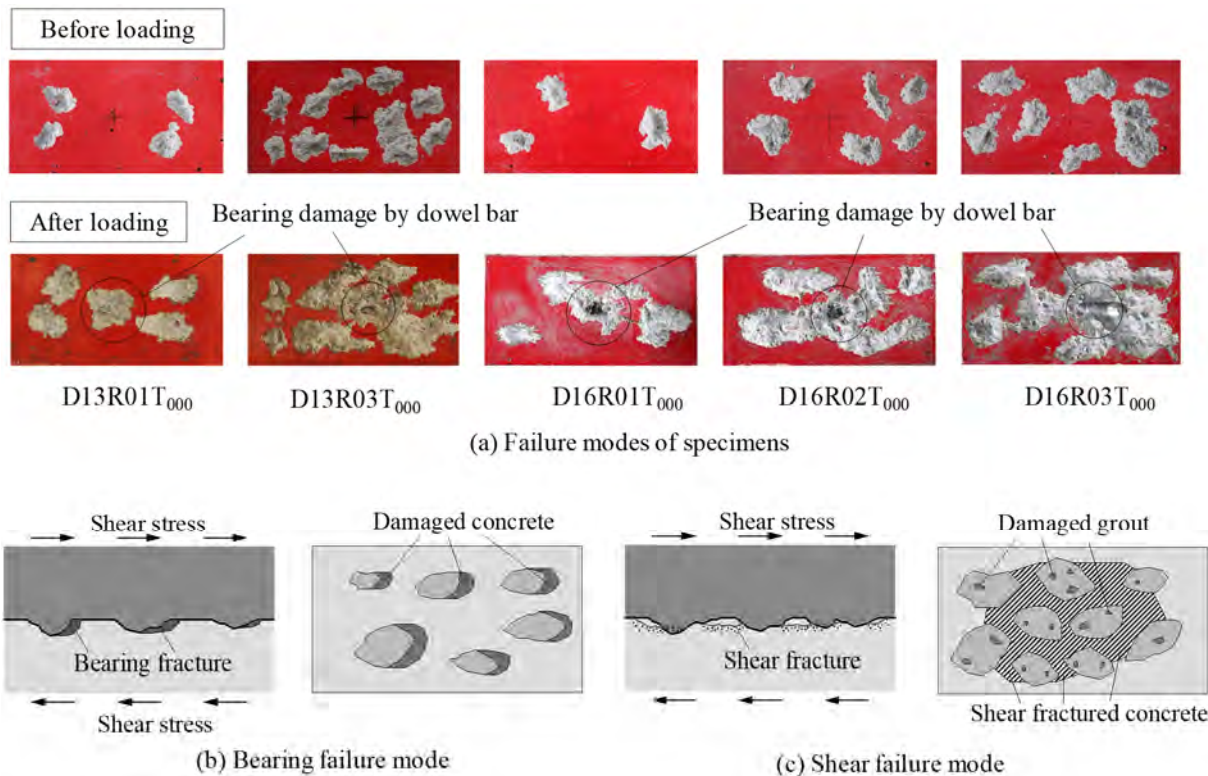


Fig. 4 Failure modes (Takase and Yamada 2022).

Table 2 Maximum shear forces in the tests.

Specimen ID	r_N	d_d	r_{rc}	$+\delta_{max}$ (mm)	$+Q_{max}$ (kN)	$-\delta_{max}$ (mm)	$-Q_{max}$ (kN)	$\frac{-Q_{max}}{+Q_{max}}$
D13R01T ₀₀₀	0.00	13	0.1	0.48	51.7	-0.45	-53.7	1.04
D13R01T ₀₃₃	0.33			0.47	57.8	-0.42	-42.6	0.74
D13R01T ₀₆₆	0.66			0.48	28.7	-0.50	-26.6	0.93
D13R02T ₀₀₀	0.00		0.2	0.20	82.8	-0.27	-76.9	0.93
D13R02T ₀₃₃	0.33			0.43	61.1	-0.26	-55.5	0.91
D13R02T ₀₆₆	0.66			0.46	33.9	-0.25	-32.7	0.96
D13R03T ₀₀₀	0.00		0.3	0.24	126.1	-0.24	-118.6	0.94
D13R03T ₀₃₃	0.33			0.50	72.0	-0.39	-69.7	0.97
D13R03T ₀₆₆	0.66			0.25	47.8	-0.25	-49.7	1.04
D16R01T ₀₀₀	0.00	16	0.1	0.95	61.4	-0.50	-56.9	0.93
D16R01T ₀₃₃	0.33			0.49	62.0	-0.50	-67.1	1.08
D16R01T ₀₆₆	0.66			0.48	35.1	-0.25	-37.0	1.05
D16R02T ₀₀₀	0.00		0.2	0.48	115.1	-0.25	-93.8	0.81
D16R02T ₀₃₃	0.33			0.50	74.7	-0.24	-86.3	1.16
D16R02T ₀₆₆	0.66			0.50	45.3	-0.25	-44.4	0.98
D16R03T ₀₀₀	0.00		0.3	0.48	167.8	-0.25	-142.9	0.85
D16R03T ₀₃₃	0.33			0.41	120.2	-0.25	-97.0	0.81
D16R03T ₀₆₆	0.66			0.21	73.9	-0.70	-33.4	0.45
D19R01T ₀₀₀	0.00	19	0.1	0.95	104.5	-0.49	-99.3	0.95
D19R01T ₀₃₃	0.33			0.39	75.7	-1.00	-57.1	0.75
D19R01T ₀₆₆	0.66			0.88	42.8	-0.50	-42.5	0.99
D19R02T ₀₀₀	0.00		0.2	0.25	155.2	-0.25	-130.0	0.84
D19R02T ₀₃₃	0.33			0.93	96.4	-0.49	-89.8	0.93
D19R02T ₀₆₆	0.66			0.47	47.8	-0.49	-41.7	0.87
D19R03T ₀₀₀	0.00		0.3	0.25	154.6	-0.25	-142.3	0.92
D19R03T ₀₃₃	0.33			0.50	108.5	-0.50	-107.2	0.99
D19R03T ₀₆₆	0.66			0.47	65.4	-0.25	-62.8	0.96
Average				0.49	—	-0.38	—	0.91

explained. **Table 2** lists the maximum shear loads used in the tests. $+Q_{max}$ and $-Q_{max}$ are the maximum shear force on the positive and negative sides, respectively. In addition, $+\delta_{max}$ and $-\delta_{max}$ are the shear displacements during $+Q_{max}$ and $-Q_{max}$, respectively.

According to **Table 2**, the range of $+\delta_{max}$ and $-\delta_{max}$ are 0.20 to 0.95 and -0.24 to -1.00, respectively. For most specimens, the values of δ at the peak load were 0.5 mm or less. Moreover, as r_N increased, the values of $+Q_{max}$ and $-Q_{max}$ decreased. This trend was observed because the resistance performances of the dowel bars and surfaces also reduced owing to the tensile stress. However, with larger d_d or r_{rc} , the bearing areas around the dowel bar and uneven surface also enlarged, respectively. Therefore, the values of $+Q_{max}$ and $-Q_{max}$ increased.

Focusing on the ratio of $-Q_{max}$ to $+Q_{max}$, the range was between 0.74 and 1.16. Although the strength on the negative side was generally smaller than that on the positive side, $-Q_{max}$ was larger than $+Q_{max}$ for certain specimens. The average of the ratio was 0.91; therefore, as a characteristic of all specimens, $-Q_{max}$ was approximately 0.9 times of $+Q_{max}$.

3.3 Shear load-slip curves

Figure 5 shows the shear load-slip (Q - δ) curves of the

test and dowel model (Takase 2019; Matsunaga *et al.* 2021, 2022) with $d_d = 16$ mm and $r_{rc} = 0.2$. As shown in this figure, “Exp.” and “Dowel” indicate the test results and the analytical results obtained by the dowel model.

As shown in **Fig. 5** and **Table 2**, the values of Q peak at $\delta = 0.25$ -0.50 mm on both the positive and negative sides; subsequently, Q decreases. After $\delta = 1.5$ -2.0 mm, Q attains a constant value. In addition, the energy assumptions for the second and fourth quadrants were small. Comparing the test results with the dowel model, where δ is smaller, the differences between the test results and the dowel model are significant. With an increase in δ , the differences decrease. Additionally, for the specimen with $r_N = 0.33$ or 0.66, the test results almost correspond with the dowel model after $\delta = 2.0$ mm; thus, under these conditions, the roughened surface could not resist the shear force.

The differences between the test results and dowel model can be regarded as the mechanical behavior of the roughened surface. Therefore, to estimate the Q - δ curves, a mechanical model of the roughened surface was constructed based on the test results in this study.

4. Mechanical model for estimating cyclic behavior

In this study, the mechanical behaviors of the previous tests were estimated by combining the dowel and roughened surface models. To estimate cyclic behavior, the previous dowel model was used, while a roughened surface model was proposed in this study. This section explains the model in detail.

4.1 Previous dowel model (Takase 2019; Matsunaga et al. 2021, 2022)

The dowel model has been proposed in previous studies. In this section, the proposed dowel model is briefly outlined. **Figure 6** shows an image of the dowel model.

The shear force Q_d is expressed as follows:

$$Q_d = q_s + q_B + q_T^S \quad (2)$$

where q_s is the shear force owing to the bending moment of the plastic hinge; q_B is the integral value of the bearing stress; q_T^S is the shear force exerted by the catenary action; and q_s , q_B , and q_T^S are calculated using M_s , σ_b , and σ_t , respectively, as illustrated in **Fig. 6**. The cyclic behavior of M_s is based on the Menegotto-Pinto (1973) model. Moreover, as shown in **Fig. 6**, the cyclic behavior of σ_b can be estimated using this model.

4.2 Envelope curve of the roughened surface

As previously mentioned, Isozaki *et al.* (2018) proposed a mechanical model of a roughened surface. However, the contact density function and contact stress model were used in the model; therefore, it was difficult to apply the model to evaluate the behavior subjected to tensile and shear stresses. Hence, in this study, the envelope model proposed in a previous paper (Yamada *et al.* 2022) is used, and the details of the model are as follows.

Based on the test results, bearing failure was observed

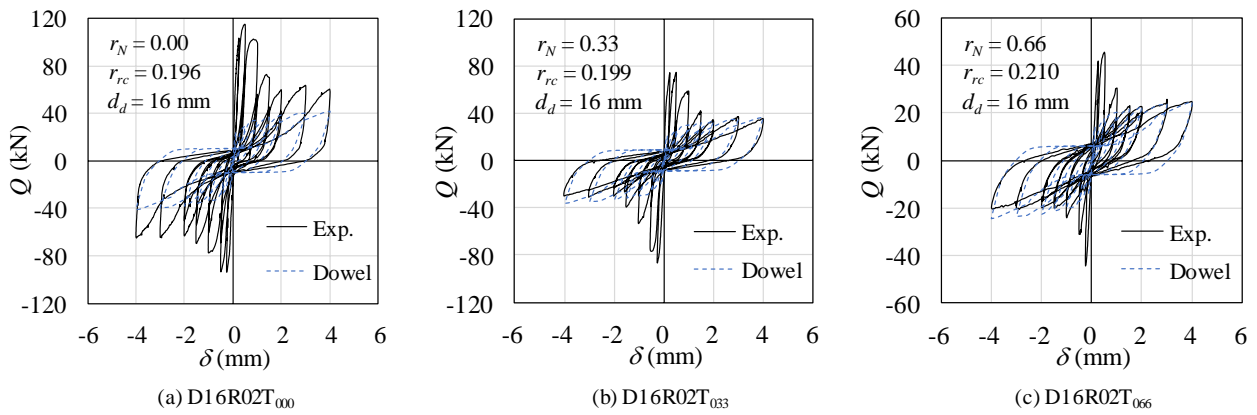


Fig. 5 Q - δ curves of the test and dowel model with $d_d = 16$ mm and $r_{rc} = 0.2$.

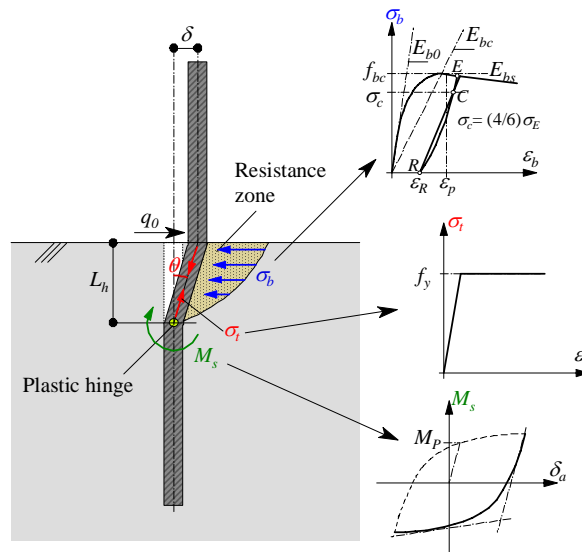


Fig. 6 Image of the dowel model. σ_b is the bearing stress of concrete, M_s is the full plastic bending moment at the plastic hinge, and σ_t is the tensile stress of the anchor bolt owing to catenary action (Takase 2019; Matsunaga *et al.* 2021, 2022).

as described in Section 3.1. A bearing failure can be regarded as a local compressive failure. Therefore, to estimate the envelope curves of the roughened surface, the Saenz model (1964), a constitutive model of concrete, was applied. The model is described as follows:

$$\sigma = \frac{E_{b0} \cdot \varepsilon}{1 + \left(\frac{E_{b0}}{E_{bc}} - 2 \right) \left(\frac{\varepsilon}{\varepsilon_{cp}} \right) + \left(\frac{\varepsilon}{\varepsilon_{cp}} \right)^2} \quad (3)$$

where σ and ε are the compressive stress and strain, respectively, and E_{b0} and E_{bc} are the initial stiffness and angle of the line through the original and peak points, respectively. ε_{cp} is the strain during the peak. Here, for applying Eq. (3) to the τ_{rc} - δ curve of the roughened surface, the symbols are changed as follows:

$$\tau_{rc} = \frac{G_{b0} \cdot \delta}{1 + \left(\frac{G_{b0}}{G_{bc}} - 2 \right) \left(\frac{\delta}{\delta_{cp}} \right) + \left(\frac{\delta}{\delta_{cp}} \right)^\beta} \quad (4)$$

where G_{b0} and G_{bc} are the initial stiffness and angle of the line passing through the original and peak points, respectively. From the test results, $G_{b0} = 6.9 \text{ N/mm}^2/\text{mm}$ and $\delta_{cp} = 0.50 \text{ mm}$ are used. **Figure 7** shows the envelope curve.

In the original model, using Eq. (3), $\beta = 2$ was employed. The stress-softening behavior can be changed by

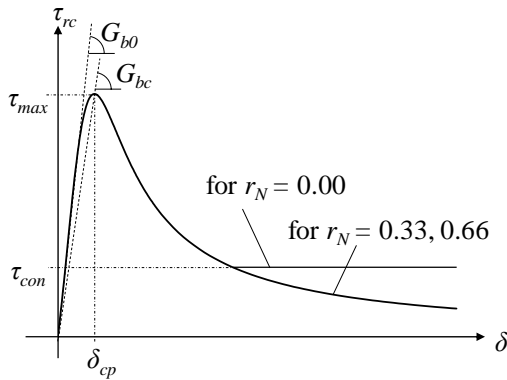


Fig. 7 Modeling of envelope curve.

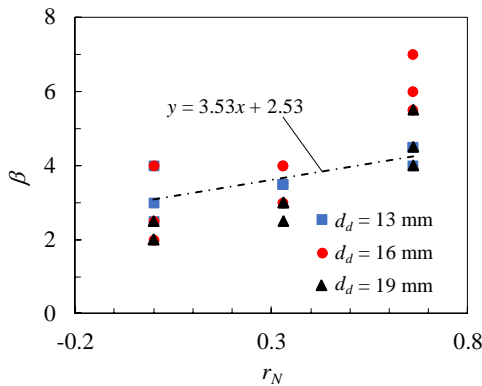


Fig. 8 Relationship between β and r_N .

tuning β . According to the test results shown in **Fig. 5**, as r_N increased, the inclination of the stress softening increased. In addition, **Fig. 8** depicts the relation between β - r_N . The values of β were obtained by the regression analysis with $\delta = 0.4 \text{ mm}$ for all specimens. From this analysis, the following equation is used:

$$\beta = 3.5 \cdot r_N + 2.5 \quad (5)$$

Moreover, for the specimen with $r_N = 0.00$, Q converged to a constant value. Therefore, the following condition is employed:

$$\tau_{con} = 0.3, \text{ where } \delta > \delta_{cp} \quad (6)$$

where τ_{con} is the constant shear stress after softening. It is obtained from the average stress with $\delta = 2.6 \text{ mm}$ for specimens with $r_N = 0.00$.

Furthermore, the authors proposed a shear strength formula in a previous study (Takase and Yamada 2022). The uneven surface was regarded as a cone. Moreover, the shear strength τ_{max} was affected by the vertical projection area of the uneven surface and the value of the exponent of f_c (Musya *et al.* 2019). Then, by the regression analysis, the value of $\tau_{max,p}$ is expressed by the following equation:

$$\tau_{max,p} = \left(\frac{r_{rc} D_{max}}{3\sqrt{\pi}} f_c^{0.24} + 0.13 \right) (1 - r_N) \quad (7)$$

where $\tau_{max,p}$ is the maximum shear stress on the positive side, and D_{max} is 12.6 mm (**Table 1**). The function of $(1 - r_N)$ represents a reduction coefficient introduced by the tensile stress.

Moreover, from **Table 2**, the maximum shear load on the negative side $\tau_{max,n}$ is smaller than $\tau_{max,p}$. Therefore, $\tau_{max,n}$ is calculated using the following equation:

$$\tau_{max,n} = 0.9 \times \tau_{max,p} \quad (8)$$

Here, **Fig. 9** illustrates the comparison of shear strength between the test results and the calculated values

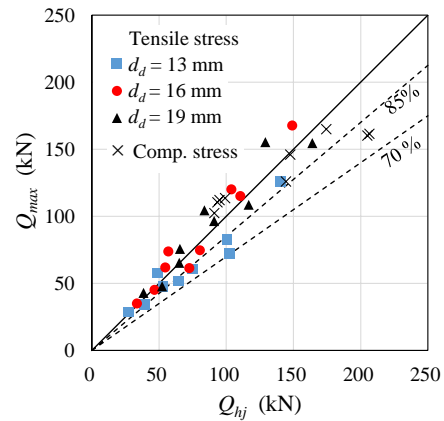


Fig. 9 Comparison of shear strength between the test and calculated results (Takase and Yamada 2022). Q_{max} is the same as $+Q_{max}$ of this study.

Q_{hj} (Takase and Yamada 2022). Q_{hj} is calculated as follows:

$$Q_{hj} = \tau_{max,p} \times A_j + Q_{d,ave} \quad (9)$$

In addition, $Q_{d,ave}$ is obtained by Eq. (2), with $\delta = 0.46$ mm, which is the average shear displacement during Q_{max} . Q_{max} is the same as the $+Q_{max}$ of this study. According to **Fig. 9**, Q_{hj} nearly matches $+Q_{max}$; however, for $d_d = 13$ mm, Q_{hj} causes the overestimation of the test results for some specimens. **Figure 10** displays the relation between the ratio of $+Q_{max}$ to Q_{hj} and w_{max} , where w_{max} indicates the opening width of the interface during $+Q_{max}$. As observed in the relation, as w_{max} increases, the ratio of $+Q_{max}/Q_{hj}$ decreases. Furthermore, focusing on w_{ave} , which is the average of w_{max} , the w_{ave} with $d_d = 13$ mm is the widest. Considering aggregate interlocking, the opening width increases and the shear stress decreases (Bujadham and Maekawa 1992a, 1992b). Thus, with d_d smaller, the opening widths marginally increased because the tensile resistance was weakened. Therefore, we concluded that the shear resistance of the roughened surface reduced with $d_d = 13$ mm.

4.3 Cyclic behavior

Figure 11 shows an image of the cyclic model. Point B and C represent the starting and end points of the unloading curve, respectively. Point Z is the cross-point of the unloading and reloading curves. In the proposed model, the unloading behavior is expressed using a parabolic function through Point B and C. δ_c , the shear displacement of Point C, is expressed using δ_B .

$$\delta_c = 0.9 \cdot \delta_B \quad (10)$$

With Point C being a vertex, the parabolic function for evaluating the unloading behavior can be described as follows:

$$\tau_{rc} = \gamma(\delta - \delta_c)^2 \quad (11)$$

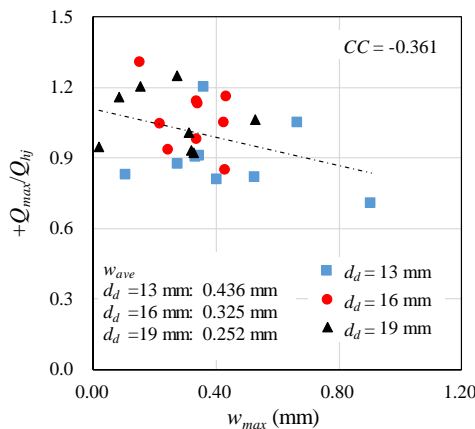


Fig. 10 Relationship between $+Q_{max}/Q_{hj}$ and w_{max} . CC represents the correlation coefficient.

$$\gamma = \frac{\tau_B}{(0.1 \cdot \delta_B)^2} \quad (12)$$

Subsequently, the reloading behavior is explained. The reloading behavior starts from the original Point O; thereafter, the reloading behavior is expressed linearly through Point O and Z, with Point Z being the point where the shear stress becomes half of τ_B .

$$\tau_Z = 0.5\tau_B \quad (13)$$

Using Point Z, the reloading behavior can be expressed by the following equation:

$$\tau_{rc} = \frac{\tau_Z}{\delta_Z} \cdot \delta \quad (14)$$

After the reloading line expressed by Eq. (14) crosses the envelope curve, τ_{rc} can be calculated using Eq. (4). Finally, the analytical shear load Q_{Ana} is calculated as follows:

$$Q_{Ana} = Q_d + Q_{rc} \quad (15)$$

$$Q_{rc} = A_j \times \tau_{rc} \quad (16)$$

5. Discussion

In this section, the analytical values of the proposed model are compared with the test results.

5.1 Q-δ curves

Figures 12 to 14 compares the test results with the analytical results for $d_d = 13, 16$, and 19 mm, respectively. These figures illustrate the results of the dowel model calculated by Eq. (2).

First, **Figs. 12(a), 12(d), 12(e)** and **12(h)** show that the analytical results of proposed model results are larger than the test results. However, such mismatches were not observed in **Figs. 13** and **14**. While, in **Figs. 12(b), 12(c)**,

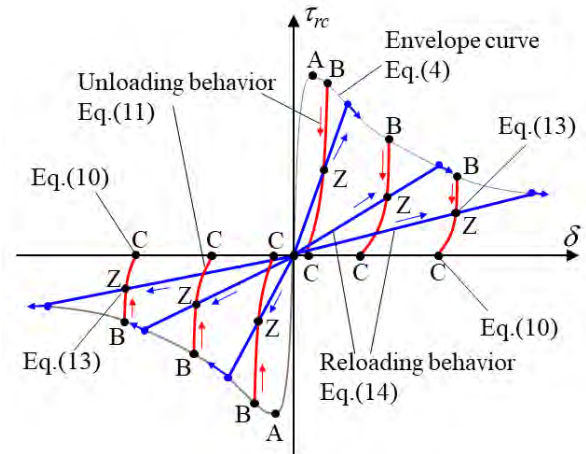


Fig. 11 Cyclic rules for the roughened surface.

12(g) and **12(i)**, the model estimated the test results suitably. As mentioned in Section 4.2, because Q_{hj} caused overestimation of the test results, the envelope curves of the model were also exaggerated. Conversely, in most actual designs of seismic retrofit building, anchors with $d_d = 16$ and 19 mm are frequently employed. Anchors with $d_d = 13$ mm are seldom used in practice and are generally used for experiments. Therefore, although some incongruence was observed for the envelope curve, the proposed model is still useful for estimating them.

Subsequently, the unloading behaviors depicted in **Fig. 12** reveal that the analytical results are in good agreement with the test results for all specimens. Thus, Eqs. (10) to (12) are appropriate for estimating the unloading behavior.

However, the accuracy of the reloading behavior is affected by the envelope curves. Therefore, the results of the reloading behaviors of the model are larger than the test results, as shown in **Figs. 12(a)** and **12(g)**. In contrast, in **Figs. 12(f)** and **12(i)**, the model results were smaller than the test results for the reloading behavior. Whereas, the test results shown in **Figs. 12(b)**, **12(c)** and **12(d)** are suitably predicted. Therefore, although there are some mismatches, the model can reasonably estimate the reloading behaviors.

Subsequently, **Figs. 13** and **14** show the envelope curves of the analytical results that are in good agreement with the test results for most of the specimens. Notably, the model produces inaccurate results for certain specimens owing to the arbitrary morphology of their surfaces.

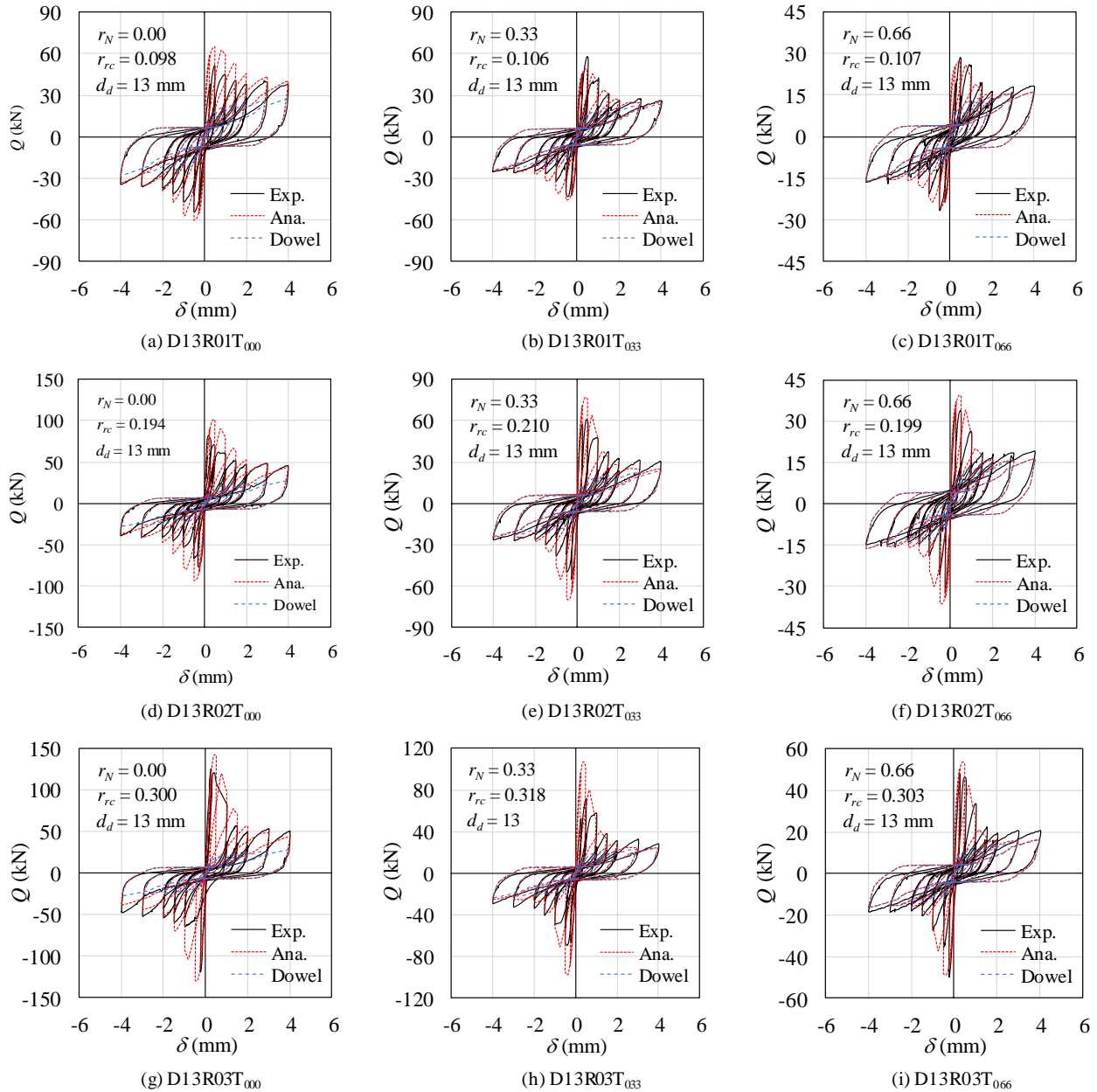


Fig. 12 Comparison of test results among the model for $d_d = 13$ mm.

Table 3 Ratio of shear load R_Q ($R_Q = Q_{Exp}/Q_{Ana}$).

Specimen ID	δ (mm) on the positive side						δ (mm) on the negative side					
	+0.25	+0.5	+1	+2	+3	+4	-0.25	-0.5	-1	-2	-3	-4
D13R01T ₀₀₀	0.65	0.79	0.77	0.84	0.92	0.94	0.90	0.89	0.83	0.94	1.00	1.03
D13R01T ₀₃₃	1.01	1.17	1.09	0.99	1.13	1.05	0.99	0.93	0.83	0.91	1.04	1.01
D13R01T ₀₆₆	0.76	1.04	1.18	1.05	1.16	1.13	0.98	1.04	0.95	0.89	1.09	1.01
D13R02T ₀₀₀	0.89	0.69	0.76	0.91	1.00	1.04	0.93	0.72	0.69	0.88	1.00	1.07
D13R02T ₀₃₃	0.82	0.80	1.01	1.17	1.28	1.23	0.85	0.73	0.84	0.97	1.10	1.05
D13R02T ₀₆₆	0.92	0.86	1.07	1.15	1.18	1.18	0.96	0.72	0.54	0.89	0.66	0.92
D13R03T ₀₀₀	1.05	0.76	0.85	0.90	1.11	1.17	1.07	0.42	0.69	1.04	1.18	1.23
D13R03T ₀₃₃	0.56	0.70	1.12	1.14	1.34	1.15	0.77	0.73	0.98	1.22	1.32	1.19
D13R03T ₀₆₆	0.96	0.89	1.27	1.22	1.32	1.28	1.09	0.74	1.05	1.01	1.17	1.11
D16R01T ₀₀₀	0.80	0.81	0.88	0.79	0.86	0.86	0.89	0.82	0.83	0.82	0.87	0.91
D16R01T ₀₃₃	1.03	1.13	1.19	0.81	0.91	0.89	1.20	1.29	1.05	0.93	0.99	0.94
D16R01T ₀₆₆	0.91	1.05	0.83	0.74	0.82	0.86	1.29	1.03	0.92	0.95	1.03	1.05
D16R02T ₀₀₀	1.06	1.04	1.10	0.91	1.02	1.04	1.03	0.90	0.89	1.04	1.17	1.27
D16R02T ₀₃₃	1.00	0.93	1.04	0.87	1.02	0.97	1.24	1.02	0.96	0.76	0.82	0.80
D16R02T ₀₆₆	1.22	1.12	1.08	1.20	1.40	1.40	1.20	0.95	0.93	1.20	1.13	1.21
D16R03T ₀₀₀	1.22	1.12	1.08	1.20	1.40	1.40	1.20	0.95	0.93	1.20	1.13	1.21
D16R03T ₀₃₃	1.10	1.11	1.01	1.10	1.31	1.19	1.09	0.67	0.92	0.92	1.02	1.00
D16R03T ₀₆₆	1.39	0.98	0.87	0.84	0.93	0.97	0.59	0.48	0.56	0.80	0.86	0.89
D19R01T ₀₀₀	1.27	1.13	1.24	1.10	1.09	1.13	1.32	1.17	1.22	1.18	1.21	1.25
D19R01T ₀₃₃	1.25	1.12	1.15	1.05	1.10	1.06	0.58	0.88	0.96	0.95	1.05	1.05
D19R01T ₀₆₆	0.72	1.01	1.16	0.95	1.04	1.09	0.74	1.06	0.98	1.05	1.14	1.16
D19R02T ₀₀₀	1.38	1.00	1.14	1.06	1.15	1.15	1.24	1.04	1.03	1.16	1.16	1.21
D19R02T ₀₃₃	0.88	1.04	1.41	1.06	1.17	1.12	1.00	1.04	0.57	1.01	1.07	0.96
D19R02T ₀₆₆	0.68	0.90	1.05	0.92	0.92	0.95	0.63	0.84	0.93	0.93	0.92	0.89
D19R03T ₀₀₀	1.11	0.87	1.08	1.17	1.29	1.31	1.10	0.90	0.98	1.13	1.12	1.14
D19R03T ₀₃₃	0.85	0.92	1.39	1.27	1.39	1.20	0.94	0.98	1.10	1.14	1.29	1.11
D19R03T ₀₆₆	0.93	1.00	1.30	1.04	1.13	1.03	1.13	0.96	1.06	1.04	1.00	1.04
Average	0.98	0.96	1.08	1.02	1.13	1.10	1.00	0.88	0.90	1.00	1.06	1.06
					Ave.	1.04					Ave.	0.98
					COV	17 %					COV	18 %

For instance, as observed in **Fig. 13(i)**, the model underestimates the shear load on the positive side and overestimates it on the negative side. As indicated in **Table 4**, $|-Q_{max}/+Q_{max}|$ is 0.45, which is the smallest of all specimens. Therefore, the authors inferred that the test results of this specimen were irregular. Thus, in the case of irregular test results, the model cannot estimate.

The unloading behaviors were accurately estimated by the model, as well as **Fig. 12**. Based on observations of the reloading curves in **Figs. 13(e), 13(f), 13(i)** and **Figs. 14(b), 14(d), 14(e), 14(f)**, it is confirmed that the model can accurately evaluate the test curves, while in other specimens, certain mismatches are observed. As mentioned earlier, the reloading accuracy is based on that of the envelope curve. Therefore, to improve the accuracy of the reloading behavior, the envelope model should be modified. However, for most specimens, the model could accurately estimate the test results of the envelope and cyclic curves. In Section 5.2, the accuracy of the model is numerically considered.

5.2 Ratio of Q_{Exp} to Q_{Ana}

Table 3 shows the ratio of R_Q that is calculated using Q_{Exp}/Q_{Ana} ; where, Q_{Exp} and Q_{Ana} are the shear forces of the test and analytical results, respectively.

First, the positive side is focused on. The range of R_Q is 0.56-1.41. As mentioned in Section 5.1, the model

overestimated for certain specimens with $d_d = 13$ mm. Therefore, the range of R_Q with $d_d = 13$ mm and $\delta = 0.25$ mm is 0.56-0.82 for D13R01T₀₀₀, D13R01T₀₆₆, D13R02T₀₃₃, and D13R03T₀₃₃. However, for all specimens, the average values with $\delta = 0.25$ -4 mm are 0.98, 0.96, 1.08, 1.02, 1.13, and 1.10, respectively. Therefore, no significant difference was confirmed, even when δ was different. In addition, the average of R_Q of all specimens was 1.04; the coefficient of variation COV is 17%. From these results, the proposed model can accurately estimate the envelope curves of most specimens on the positive side.

Subsequently, the negative side is explained. The range of R_Q is 0.42-1.32. The R_Q values of D13R03T₀₀₀ and D16R03T₀₆₆ with $\delta = 0.5$ mm are 0.42 and 0.48, respectively; thus, the model overestimated the test results. Therefore, the peak forces were considered to be affected by the failure on the positive side. However, the average values with $\delta = -0.25$ to -4 mm were 1.00, 0.88, 0.90, 1.00, 1.06, and 1.06, respectively. In addition, the average value of all the specimens was 0.98; COV was 18%. Therefore, in addition to the positive side, the model reasonably estimated the test results for all specimens.

Next, the accuracy of reloading is discussed. **Table 4** lists the estimation results of the ratio of $R_{Q,r}$, which is R_Q for reloading. The values listed in the table correspond to Point Z of **Fig. 11**. The values of $R_{Q,r}$ with $\delta = +0.25$ and

−0.25 mm are 0.33-1.10 and 0.20-0.96, respectively; the average values were 0.67 and 0.59, respectively. Thus, the model significantly overestimated the test results. As mentioned in Section 5.1, the accuracy for reloading was affected by the accuracy for the envelope curves. Therefore, $d_d = 13$ mm, the value of $R_{Q,r}$ was inaccurate. However, after ± 0.5 mm, the accuracies improved; the average values were 0.82 to 1.07. Here, for D13R03T₀₀₀ and D16R03T₀₃₃, $R_{Q,r}$ with $\delta = +0.5$ mm were extremely small, 0.13 and 0.28, respectively. For this reason, when $\delta = +0.5$ mm, large slips were observed in these specimens. Therefore, the shear forces of the reloading at $\delta = +0.5$ mm were minute. Hence, the proposed model cannot estimate the reloading behavior after a large slip.

As mentioned above, although a few irregular cases

were observed, the modeling for reloading behavior was largely accurate.

5.3 Ratio of Q_d to Q_{Ana}

Table 5 lists the ratio of R_d that is obtained by Q_d/Q_{Ana} ; where, Q_d is the shear force of the dowel model. Based on these results, the ratio of dowel action to the analytical result is discussed.

The range of R_d with $\delta = +0.25$ and -0.25 mm is 0.12-0.55 and 0.13-0.57, respectively, whereas the range of R_d with $\delta = +4$ and -4 mm is 0.62-1.00 and 0.71-1.00, respectively. From the results, when the value of δ is small, the effect of the roughened surface is significant; however, when δ is greater, it becomes insignificant. In particular, when the value of δ is greater than 3 mm with r_N

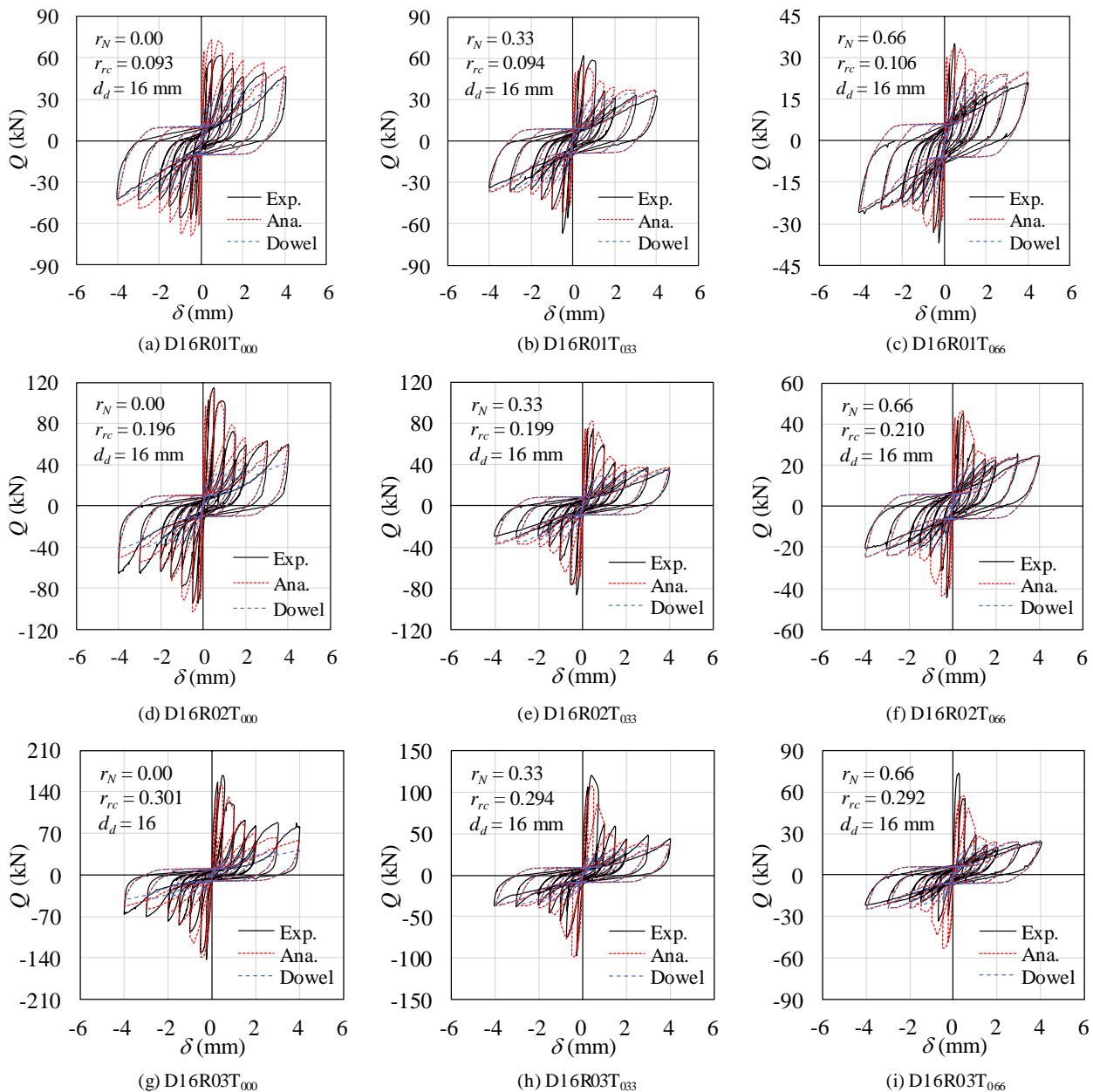


Fig. 13 Comparison test results with model for $d_d = 16$ mm.

$= 0.33$ or 0.66 , the value of R_d is greater than 0.91 on both sides. In summary, when the surface is subjected to shear and tensile forces, the shear loads are resisted only by dowel action at larger shear displacements. For the specimens with $r_N = 0.00$, the range of R_d is 0.62 - 0.84 with $\delta = 4$ mm. Therefore, when the surface is not subjected to tensile force, it can resist the shear force in a large shear displacement. Moreover, when d_d is small, R_d also becomes small, whereas when r_{rc} is small, R_d is large.

Observing R_d of D13R01T₀₀₀ and D13R01T₀₆₆ with $\delta = +0.25$ mm, the values are 0.25 and 0.34 , respectively. Thus, when r_N increases from 0.00 to 0.66 , R_d is approximately 1.5 times. Similar characteristics were observed for other specimens. Therefore, as r_N increases, the effect

of the dowel bars becomes more significant.

As described before, when interfaces are used with a small slip, mainly the structural design of roughened surfaces becomes crucial, whereas when interfaces are used with a large slip, mainly the design of dowel bars becomes important.

6. Conclusions

In this study, the envelope and cyclic behaviors of roughened concrete surfaces were modeled by incorporating the previous dowel model to estimate the previous test results (Takase and Yamada 2022). The findings of this study are as follows:

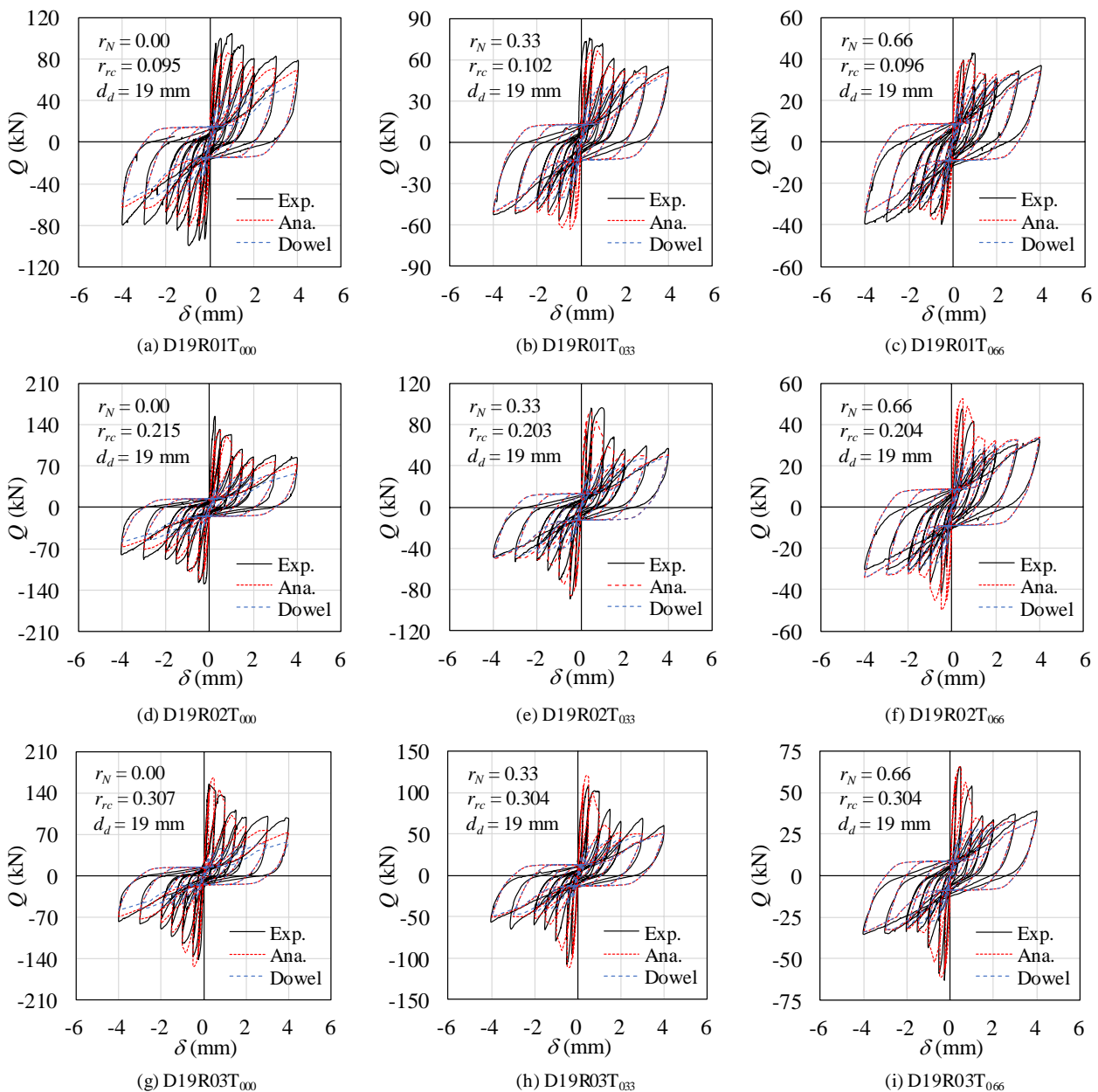


Fig. 14 Comparison test results with model for $d_d = 19$ mm.

Table 4 Ratios of shear load $R_{Q,r}$ ($R_{Q,r} = Q_{Exp}/Q_{Ana}$ for reloading).

Specimen ID	δ (mm) on the positive side						δ (mm) on the negative side					
	+0.25	+0.5	+1	+2	+3	+4	-0.25	-0.5	-1	-2	-3	-4
D13R01T ₀₀₀	0.42	0.66	0.67	0.87	0.87	0.84	0.94	1.16	1.06	1.12	0.95	0.86
D13R01T ₀₃₃	0.76	1.05	0.80	0.98	1.03	0.97	0.64	1.05	0.87	1.00	1.06	0.91
D13R01T ₀₆₆	0.48	0.79	0.80	1.07	1.05	1.02	0.74	0.99	0.81	0.96	1.02	1.02
D13R02T ₀₀₀	0.58	0.90	0.83	1.00	0.87	0.81	0.52	1.00	0.90	1.03	0.83	0.76
D13R02T ₀₃₃	0.40	0.60	0.76	1.11	1.03	1.02	0.53	0.95	0.88	1.06	1.08	0.99
D13R02T ₀₆₆	0.54	0.60	0.77	1.13	1.17	1.09	0.32	0.49	0.69	0.97	0.94	0.88
D13R03T ₀₀₀	0.68	0.13	0.54	0.88	0.89	0.89	0.39	0.31	0.82	1.27	0.94	0.84
D13R03T ₀₃₃	0.33	0.59	0.67	0.96	0.93	0.90	0.57	1.02	0.79	1.16	1.05	0.94
D13R03T ₀₆₆	0.36	0.45	0.80	1.25	1.19	1.14	0.41	0.74	0.89	1.15	1.10	1.03
D16R01T ₀₀₀	0.71	0.98	0.89	0.83	0.76	0.76	0.49	1.04	1.04	0.97	0.83	0.83
D16R01T ₀₃₃	0.77	1.05	0.65	1.01	0.86	0.85	0.77	1.39	1.01	1.13	0.88	0.88
D16R01T ₀₆₆	0.44	0.52	0.61	0.83	0.88	0.89	0.70	0.70	0.87	1.04	1.07	1.00
D16R02T ₀₀₀	0.88	1.15	0.92	0.89	0.81	0.79	0.59	1.12	1.14	1.18	0.89	0.92
D16R02T ₀₃₃	0.46	0.62	0.68	0.81	0.87	0.83	0.73	0.84	0.80	0.73	0.80	0.78
D16R02T ₀₆₆	0.81	0.96	0.99	1.17	1.08	1.04	0.49	0.94	1.15	1.34	0.91	0.75
D16R03T ₀₀₀	0.81	0.96	0.99	1.17	1.08	1.04	0.49	0.94	1.15	1.34	0.91	0.75
D16R03T ₀₃₃	0.89	0.28	0.68	0.84	0.87	0.87	0.38	0.29	0.86	0.77	0.77	0.78
D16R03T ₀₆₆	0.68	0.42	0.65	0.90	0.97	0.99	0.20	0.21	0.65	0.82	0.92	0.87
D19R01T ₀₀₀	1.04	1.35	1.42	1.20	1.09	0.99	0.96	1.40	1.44	1.30	1.10	1.02
D19R01T ₀₃₃	1.10	1.17	1.07	1.05	1.06	1.01	0.33	0.91	1.00	1.03	1.06	1.01
D19R01T ₀₆₆	0.54	0.97	0.92	1.02	1.09	1.07	0.82	1.18	0.97	1.13	1.22	1.16
D19R02T ₀₀₀	0.84	1.26	1.15	1.08	1.03	1.05	0.83	1.43	1.35	1.28	1.07	0.98
D19R02T ₀₃₃	0.66	1.22	1.00	0.98	0.96	0.95	0.70	1.24	1.09	0.92	0.97	0.94
D19R02T ₀₆₆	0.63	0.74	0.74	0.96	0.99	0.99	0.47	0.71	0.83	0.99	0.89	0.91
D19R03T ₀₀₀	1.01	1.00	1.08	1.21	1.23	1.17	0.79	1.28	1.31	1.26	1.04	1.01
D19R03T ₀₃₃	0.65	1.08	1.03	1.04	1.01	1.00	0.46	1.06	1.00	1.01	1.02	0.99
D19R03T ₀₆₆	0.66	0.70	0.83	1.07	1.13	1.13	0.59	0.69	0.97	1.03	1.07	1.07
Average	0.67	0.82	0.85	1.01	0.99	0.97	0.59	0.93	0.98	1.07	0.98	0.92
Ave.						0.89						0.91
COV						25 %						27 %

- 1) In the proposed cyclic model of roughened concrete surfaces, the envelope curves were first modeled using the Saenz model (1964). The maximum shear stress on the positive side ($\tau_{max,p}$) was calculated using a previous expression (Takase and Yamada 2022). Moreover, the peak stress on the negative side ($\tau_{max,n}$) was 0.9 times as $\tau_{max,p}$.
- 2) For specimens with $d_d = 13$ mm, the model overestimated the envelope curves. The authors assumed that the opening width marginally wider for a smaller d_d ; therefore, the shear resistance of the surface reduced. However, the average ratio and COV of Q_{Exp}/Q_{Ana} were 1.04 and 0.98, 17% and 18% on the positive and negative sides, respectively; the envelope curves were reasonably evaluated by the proposed model for most of the specimens.
- 3) In the roughened surface model, the unloading behavior was modeled using a parabolic function, whereas the reloading behavior was modeled using a linear function across Points O and Z, as shown in Fig. 11. The unloading and reloading behaviors were effectively estimated by modeling.
- 4) When δ is small, the shear forces are mainly resisted by the roughened surface because the range of R_d with $\delta = +0.25$ and -0.25 mm was 0.12-0.55 and 0.13-0.57, while that with $\delta = +4$ and -4 mm was 0.62-1.00 and 0.71-1.00; therefore, as δ increases, the effect of the

- dowel bars intensifies. In addition, with an increase in r_N or d_d , the value of Q_d divided by Q_{Ana} , that is, R_d , increased. By contrast, when r_N is large, R_d decreased.
- 5) The proposed model could be applied for $r_N = 0.1$ -0.3, $f_c = 20$ -23 N/mm², $d_d = 13$ -19 mm, and $r_N = 0.00$ -0.66 similar to that in the previous study (Takase and Yamada 2022).

Overall, the mechanical behavior of interfaces comprising roughened surfaces and dowel bars can be reasonably estimated by the proposed model. Indeed, the model accuracy for $d_d = 13$ mm should be improved. However, because anchors with 16 and 19 mm are employed to actual seismically retrofitted buildings, the findings of this research can facilitate their structural design and analysis. In addition, the case of $d_d > 20$ mm should be further investigated.

Finally, the bearing failure mode was modeled in this study. Future studies will focus on the shear failure mode; therefore, specimens with other f_c and r_N will be tested.

Acknowledgments

This study was supported by the Japan Society for the Promotion of Science KAKENHI (grant number JP19K04684), and partially supported by the Collaborative Research Project of the Laboratory for Materials and Structures, Institute of Innovative Research, Tokyo Institute of Technology.

Table 5 Ratio of dowel action R_d , ($R_d = Q_d/Q_{Ana}$).

Specimen ID	δ (mm) on the positive side						δ (mm) on the negative side					
	+0.25	+0.5	+1	+2	+3	+4	-0.25	-0.5	-1	-2	-3	-4
D13R01T ₀₀₀	0.25	0.28	0.36	0.54	0.59	0.67	0.27	0.30	0.38	0.63	0.73	0.82
D13R01T ₀₃₃	0.28	0.32	0.48	0.79	0.91	0.96	0.30	0.34	0.49	0.79	0.92	0.96
D13R01T ₀₆₆	0.34	0.39	0.58	0.92	0.98	0.99	0.37	0.42	0.60	0.92	0.98	0.99
D13R02T ₀₀₀	0.17	0.18	0.27	0.47	0.54	0.62	0.18	0.20	0.29	0.52	0.63	0.75
D13R02T ₀₃₃	0.18	0.21	0.40	0.78	0.91	0.96	0.20	0.23	0.41	0.78	0.91	0.96
D13R02T ₀₆₆	0.24	0.27	0.52	0.92	0.98	0.99	0.26	0.30	0.53	0.92	0.98	0.99
D13R03T ₀₀₀	0.12	0.13	0.22	0.44	0.54	0.62	0.13	0.14	0.23	0.48	0.59	0.71
D13R03T ₀₃₃	0.14	0.15	0.36	0.77	0.91	0.96	0.15	0.17	0.37	0.77	0.91	0.96
D13R03T ₀₆₆	0.18	0.21	0.48	0.92	0.98	0.99	0.19	0.22	0.49	0.92	0.98	0.99
D16R01T ₀₀₀	0.36	0.40	0.49	0.65	0.70	0.77	0.39	0.42	0.51	0.74	0.81	0.88
D16R01T ₀₃₃	0.41	0.46	0.61	0.86	0.94	0.97	0.44	0.49	0.62	0.86	0.94	0.97
D16R01T ₀₆₆	0.46	0.52	0.69	0.95	0.99	1.00	0.49	0.54	0.70	0.95	0.99	1.00
D16R02T ₀₀₀	0.24	0.26	0.37	0.58	0.64	0.71	0.26	0.28	0.39	0.63	0.73	0.82
D16R02T ₀₃₃	0.28	0.31	0.52	0.85	0.94	0.97	0.30	0.34	0.53	0.85	0.94	0.97
D16R02T ₀₆₆	0.33	0.37	0.63	0.95	0.99	1.00	0.35	0.40	0.64	0.95	0.99	1.00
D16R03T ₀₀₀	0.19	0.20	0.31	0.55	0.64	0.71	0.20	0.21	0.33	0.59	0.69	0.79
D16R03T ₀₃₃	0.22	0.24	0.48	0.84	0.94	0.97	0.23	0.26	0.49	0.84	0.94	0.97
D16R03T ₀₆₆	0.27	0.31	0.60	0.95	0.99	1.00	0.29	0.33	0.61	0.95	0.99	1.00
D19R01T ₀₀₀	0.42	0.47	0.56	0.72	0.76	0.82	0.45	0.49	0.58	0.79	0.85	0.91
D19R01T ₀₃₃	0.46	0.52	0.67	0.89	0.96	0.98	0.49	0.54	0.68	0.89	0.96	0.98
D19R01T ₀₆₆	0.55	0.61	0.76	0.96	0.99	1.00	0.57	0.63	0.77	0.96	0.99	1.00
D19R02T ₀₀₀	0.28	0.30	0.43	0.65	0.71	0.77	0.30	0.33	0.45	0.69	0.77	0.85
D19R02T ₀₃₃	0.33	0.37	0.59	0.88	0.96	0.98	0.35	0.40	0.61	0.88	0.96	0.98
D19R02T ₀₆₆	0.39	0.45	0.70	0.96	0.99	1.00	0.42	0.48	0.71	0.96	0.99	1.00
D19R03T ₀₀₀	0.23	0.24	0.38	0.63	0.71	0.77	0.24	0.26	0.40	0.66	0.75	0.84
D19R03T ₀₃₃	0.26	0.29	0.56	0.88	0.96	0.98	0.28	0.32	0.57	0.88	0.96	0.98
D19R03T ₀₆₆	0.31	0.36	0.67	0.96	0.99	1.00	0.33	0.39	0.68	0.96	0.99	1.00

References

- Abe, T., Sakamoto, K., Hiwatashi, T., Takase, Y. and Katori, K., (2020). "Design formula for shear strength of roughened concrete by chipping." *Journal of Structural Engineering*, 66B, 517-524. (in Japanese)
- Bujadham, B. and Maekawa, K., (1992a). "Qualitative studies on mechanisms of stress transfer across cracks in concrete." *Doboku Gakkai Ronbunshu*, 451(V-17), 265-275.
- Bujadham, B. and Maekawa, K., (1992b). "The universal model for stress transfer across cracks in concrete." *Doboku Gakkai Ronbunshu*, 451(V-17), 277-287.
- Figueira, D., Sousa, C. and Neves, A. S., (2020). "Constitutive model for aggregate interlock in FEM analyses of concrete interfaces with embedded steel bars." *International Journal of Concrete Structures and Materials*, 14(2020), 15.
- Friberg, B. F., (1938). "Design of dowels in the transverse joints of concrete pavements." *Proceedings of American Society of Civil Engineers*, 64(9), 1809-1828.
- Ghayeb, H. H., Razak, H. A. and Sulong, N. H. R., (2020). "Performance of dowel beam-to-column connections for precast concrete systems under seismic loads: A review." *Construction and Building Materials*, 237, 117582.
- Isozaki, T., Musya, U., Takase, Y., Abe, T., Sakamoto, K., Hiwatashi, T. and Katori, K., (2018). "Mechanical model of shear stress transfer of roughened concrete surface for R/C existing member." In: G. Meschke, B. Pichler and J. Rots, Eds. *Proc. Conference on Computational Modelling of Concrete Structures (EURO-C 2018)*, Bad Hofgastein, Austria 26 February - 1 March 2018. London and New York: CRC Press, 973-981.
- JSA, (2011). "Metallic materials - Tensile testing - Method of test at room temperature (JIS Z 2241)." Tokyo: Japanese Standards Association. (in Japanese)
- JSA, (2018). "Method of test for compressive strength of concrete (JIS A 1108)." Tokyo: Japanese Standards Association. (in Japanese)
- Katagiri, Y., Takase, Y., Abe, T., Sakamoto, K., Hiwatashi, T. and Katori, K., (2019). "Mechanical model of roughened concrete of existing members for shear failure mode." In: G. Pijaudier-Cabot, P. Grassl and C. La Borderie, Eds. *Proc. 10th International Conference on Fracture Mechanics of Concrete and Concrete Structures (FraMCoS-10)*, Bayonne, France 23-26 June 2019. Illinois, USA: International Association for Fracture Mechanics of Concrete and Concrete Structures, 235482.
- Maekawa, K., Fukuura, N. and Soltani, M., (2008). "Path-dependent high cycle fatigue modeling of joint interfaces in structural concrete." *Journal of Advanced Concrete Technology*, 6(1), 227-242.
- Maekawa, K. and Qureshi, J., (1997). "Stress transfer across interfaces in reinforced concrete due to aggregate interlock and dowel action." *Doboku Gakkai*

- Ronbunshu*, 557(V34), 159-72.
- Matsunaga, K., Takase, Y. and Abe, T., (2021). "Modeling of dowel action for cast-in and post-installed anchors considering bond property." *Engineering Structures*, 245, 112773.
- Matsunaga, K., Takase, Y., Abe, T., Orita, G. and Ando, S., (2022). "Property of cement based adhesive anchor constructed below zero and estimating of mechanical behavior." *Journal of Structural and Construction Engineering, Transactions of AIJ*, 87(796), 556-566. (in Japanese)
- Mattock, A. H. and Hawkins, N. M., (1972). "Shear transfer in reinforced concrete recent research." *PCI Journal*, 17, 55-75.
- Menegotto, M. and Pinto, P. E., (1973). "Method of analysis for cyclically loaded R.C. plane frame including changes in geometry and non-elastic behavior of elements under combined normal force and bending." In: *Proc. IABSE Symposium on Resistance and Ultimate Deformability of Structures Acted on by Well Defined Repeated Loads*, Lisboa, Portugal 13-14 September 1973. Zurich: International Association For Bridge And Structural Engineering, 11, 15-22.
- Musya, U., Katagiri, Y., Takase, Y., Abe, T., Sakamoto, K., Hiwatashi, T. and Katori, K., (2019). "Bearing strength formula of roughened concrete considering vertical projection area." *Journal of Advanced Concrete Technology*, 17(6), 309-318.
- Saenz, L. P., (1964). "Discussion of equation for stress-strain curve of concrete." *ACI Journal*, 61(9), 1229-1235.
- Sorensen, J. H., Hoang, L. C., Olesen, J. F. and Fischer, G., (2017). "Testing and modeling dowel and catenary action in rebars crossing shear joints in RC." *Engineering Structures*, 145, 234-245.
- Takase, Y., (2019). "Testing and modeling of dowel action for a post-installed anchor subjected to combined shear and tensile forces." *Engineering Structures*, 195, 551-558.
- Takase, Y. and Yamada, T., (2022). "Shear strengths of joints with roughened concrete surfaces and post-installed dowel bars subjected to normal and shear stresses for seismically retrofitted structures." *Structures*, 45, 900-911.
- Takase, Y., Mizoguchi, M. and Wada, T., (2018). "Mechanical model of adhesive post-installed anchor subjected to combined force." In: G. Meschke, B. Pichler and J. Rots, Eds. *Proc. Conference on Computational Modelling of Concrete Structures (EURO-C 2018)*, Bad Hofgastein, Austria 26 February - 1 March 2018. London and New York: CRC Press, 955-962.
- Takase, Y., Wada, T., Ikeda, T. and Shinohara, Y., (2013). "Mechanical model of adhesive post-installed anchor subjected to cyclic shear force." In: J. G. M. Van Mier, G. Ruiz, C. Andrade, R. C. Yu and X. X. Zhang, Eds. In: *Proc. 8th International Conference on Fracture Mechanics of Concrete and Concrete Structures (FramCoS-8)*, Toledo, Spain 10-14 March 2013. Illinois, USA: International Association for Fracture Mechanics of Concrete and Concrete Structures, 1727-1736.
- Vintzileou, E. N. and Tassios, T. P., (1986). "Mathematical models for dowel action under monotonic and cyclic conditions." *Magazine of Concrete Research*, 38(134), 13-22.
- Walraven, J. C., (1981). "Fundamental analysis of aggregate interlock." *Journal of Structural Division, ASCE*, 107(11), 2245-2270.
- Walraven, J. C. and Reinhardt, H. W., (1981). "Theory and experiments on the mechanical behavior of cracks in plain and reinforced concrete subjected to shear loading." *Heron*, 26(1A), 1-68.
- Yamada, T., Takase, Y. and Abe, T., (2022). "Mechanical behavior of seismic reinforced joints using roughened surface and adhesive anchors subjected to combined stress." *Concrete Research and Technology*, 33, 33-42. (in Japanese)
- Zhang, D., Furuuchi, H., Hori, A. and Ueda, T., (2009). "Fatigue degradation properties of PCM-concrete interface." *Journal of Advanced Concrete Technology*, 7(3), 425-438.